Volume 64, Issue 1, 2020
Journal of Scientific Research
Institute of Science,
Banaras Hindu University, Varanasi, India.

Verification of Sliding Ratio (C_l/C_d) of Airfoil through CFD Analysis

P. K. Nigam[1*], Nitin Tenguria[2] and M. K. Pradhan[3]

[1]Rabindranath Tagore University, Bhopal (M. P.), India, nigam.praveen@gmail.com
[2]Sagar Institute Of Research and Technology, Bhopal (M. P.), India, tengurianitin@gmail.com
[3]Maulana Azad National Institute of Technology, Bhopal (M. P.), India, mohanrkl@gmail.com

Abstract: **Blades are very essential parts of HAWT (horizontal axis wind turbine). The lift/drag ratio is an important criteria of the aerodynamic efficiency of airfoil. In this study CFD (Computational Fluid Dynamics) analysis is performed for the verification of sliding ratio (C_l/C_d) of NACA airfoil 63(4)-221. CFD analysis is conducted at low Reynolds number in range of x105 as well as high Reynolds number in the range of x10^6. Angle of attack is taken in the range of 4º to 7º. For present work the blade length is taken 14 meters, which is a new design of blade for RRB V27-225 kW horizontal axis wind turbine blade (HAWT). Then results obtained from CFD analysis are compared with the available literature.**

Index Terms: **Horizontal Axis Wind Turbine, HAWT, CFD, ANSYS, Airfoil, Angle of attack, Sliding ratio**

I. Introduction

Wind interacts with horizontal axis wind turbine rotor and converts its kinetic energy into useful energy. Wind turbine blade undergoes various types of aerodynamic forces due to wind turbulence. An airfoil is the cross-sectional shape of a blade of wind turbine. When wind flows over an airfoil, it develops aerodynamic forces. The lift is the force component perpendicular to the direction of blade motion while drag is parallel component to the direction of motion. There are three different ways to analyze flow around wind turbine that are field testing, analytical/semi-empirical models and CFD. The first one gives precise results, but highly complex and expensive. The second is one not universally reliable, while CFD offers the best way to direct measurements.

II. Literature Survey

(Anitha et al., 2018) carried out development of wing airfoil for the efficient aerodynamic performance. The optimal shape of the airfoil produces improved lift coefficient and reduced drag within the design constraints. In this study, genetic algorithm, particle swarm optimization methods was used to the optimization of airfoil shape for airfoil NACA-4412 in software MATLAB environment. (Bartl et al., 2019) performed surface pressure, Lift and drag measurements on a wing section of the NREL-S826 wind turbine airfoil. Eight different Reynolds number taken range from 0.5×10^5 to 6.0×10^5. With the measurements of two types of Reynolds number averaged Navier-Stokes (RANS) simulations were conducted. Out of which one includes a laminar to turbulent transition model. The lift and drag behavior controlled by low Re < 0.7×10^5, that is related to the existence of laminar separation bubbles (LSBs) on the suction side of the profile. (Bianchini et al., 2016) demonstrated that, when airfoil rotates perpendicular to flow direction, it can be hypothetically transformed into an equivalent airfoil with a camber line defined by their arc of rotation. In such situation, the symmetric airfoil generally useful for Darrieus blades that actually act like virtually cambered to ensure the attended performance. To complete these analyses it was focuses on the on the aerodynamics of airfoil at the starting of the rotor. It was concluded that, symmetric airfoils shown a counter intuitive nonsymmetric starting torque over the revolution.

(Fuglsang et al., 2004) presented the designing and experimental verification of the Risø-B1 airfoil family at variable pitch control and wind speed. Seven airfoils were designed while thickness to chord ratios is taken between 15% and 53%. The airfoil was designed to gain maximum lift while maintaining high aerodynamic performance. The design optimization was carried out with a Risø in-house multi disciplinary optimization tool. Wind tunnel testing was performed for Risø-B1-18 and Risø-B1-24 in the VELUX wind tunnel, Denmark, at a R_e = 1.63106. For both airfoils the predicted target performance were achieved.

(Li et al., 2015) investigated the aerodynamic behaviour of RAE2822 in ground effect with FVM (finite volume method) based on the averaged Navier-Stokes equations. The performance of many eddy-viscosity turbulence models were assessed by comparing with the existing experimental data of NACA-4412 in ground effect. Realizable k-epsilon model showed high capability of predicting the characteristics of flow. In the study of this ground effect on airfoil RAE-2822, high lift/drag ratio can be achieved in medium AOA (angle of attack).

To gain the increased power economically through wind turbine, the aerodynamic behavior of profile of the blade must be improved. The key parameters are the lift & drag coefficient to analyze the wind-turbine blade performance. To gain the highest power from the turbine the maximum lift/drag ratio is required. (Talukder et al., 2016) performed a comparative analysis for aerodynamic performance of NREL S819 and S821 airfoils based on finite volume approach using a CFD method. Changing the angle of attack and wind speed, different aerodynamic parameters such as lift coefficient, drag coefficient and pressure distribution over the airfoils were determined computationally. The results from computations were confirmed experimentally by testing the airfoils wooden models in a wind tunnel subsonic open circuit suction type. The comparison with the experimental data indicates that the CFD approach applied in this investigation can precisely predict the aerodynamic behavior of the wind-turbine blades.

(Tenguria et al., 2017) performed CFD analysis of a blade as well as airfoil of HAWT using k-ω SST model. In this study, NACA 63(4)-221 airfoil profile was chosen for the modeling and then performs blade analysis. The lift & drag forces were find out for the blade at various AOA (angle of attack). The length of blade was taken 38.98 m, which is a redesigned blade for VESTAS V82-1.65MW HAWT blade. Results obtained from simulation were varified with the experimental work found in literature.

(Patil et al., 2015) studied the drag and lift forces of wind turbine blade at various Reynolds number and AOA. In this work NACA0012 airfoil profile was taken for analysis of blade. The drag and lift forces were find out by CFD analysis at various AOA from 0 degree to 80 degree for the Reynolds number in the range from 10000 to 800000. The validation of this work was done by comparing the result obtained from experimental results obtained by Sandia National Laboratories (SNL). It was concluded that result obtained by CFD analysis are very close with results published at SNL. (Standish et al., 2003) designed the blunt trailing edge airfoils that are especially for the large wind turbine blades inboard region. Blunt trailing edge airfoils provide improvement in lift force as well as structural benefits including easiness of manufacturing and handling. Several computational techniques were applied, including a viscous/inviscid interaction method and three Reynolds-averaged Navier-Stokes methods. (Sharma, 2016) investigated to find out the most appropriate design of airfoil for using in low speed aircrafts. The airfoil S819, S1223, S1223 and S8037 RTL was chosen for study. The CFD method was used for analysis of airfoils. The numerical simulation performed using ANSYS FLUENT for low speed and high-lift airfoil. The coefficient of moment and Lift/Drag ratio of the airfoils find out for the comparative analysis of airfoils. The S1223 RTL airfoil was selected as the most appropriate design for the Mach number from 0.10 to 0.30 and for the specified boundary conditions.

BEMT (Blade element momentum theory) is widely used for prediction of aerodynamic performance of wind turbine. But the reliability of the airfoil data is a significant aspect for the accurate prediction of power and aerodynamic forces. Mostly 2D wind tunnel tests of airfoils are done with constant span to establish the airfoil characteristics data used in BEM codes. Due to three dimensional effects, a BEM code using airfoil data received from two dimensional wind tunnel tests will not yield the correct loading and power. Consequently, two dimensional airfoil data have to be corrected before using in a BEM code. (Yang et al., 2014) considered the MEXICO rotor (Model Experiments in Controlled Conditions rotor) where airfoil data are extracted from CFD results. The comparison shows that the re-calculated forces by using airfoil data extracted from CFD have good agreements with the experiment.

In present work CFD analysis is carried out for airfoil NACA 63(4)-221 for redesigning the blade of RRB V27-225 kW HAWT. In this work the viscous spalart allmaras model is used. Spalart-Allmaras model is a one equation model which solves a transport equation for a viscosity-like variable, referred to as the Spalart-Allmaras variable. In its original form, the model is effectively a low-Reynolds number model. The Spalart–Allmaras model was developed for aerodynamic flows. The computational effort is lower compared to the commonly used two-equation models. This model is preferable in large part due to its robustness.

III. Governing Equations

The continuity equation for the two dimensional, steady and incompressible flow is

$$\nabla.(\rho V) = \frac{\partial(\rho u)}{\partial x} + \frac{\partial(\rho v)}{\partial y} = 0 \qquad (1)$$

For viscous flow in x direction the momentum equation is

$$\rho\frac{\mathrm{Du}}{\mathrm{Dt}} = \frac{\partial\rho}{\partial x} + \frac{\partial\tau_{xx}}{\partial x} + \frac{\partial\tau_{yx}}{\partial y} + \frac{\partial\tau_{zx}}{\partial z} + \rho f_{\chi} \qquad (2)$$

Where due to characteristics of the two dimensional flow in continuity equation the term $\frac{\partial(\rho w)}{\partial z}$ and in momentum equation, $\frac{\partial \tau_{zx}}{\partial z}$ drop out. In all simulations a standard *k*- ω SST model has been used for turbulent viscosity.

In equation (1) and (2)

ρ = Density of fluid,
V = Velocity vector,
ρV = Mass flux,
∇ = Vector operator,
$\nabla.(\rho V)$ = Divergence of *Pv,*
ρu, ρv = Rate of mass entering in x, y direction, respectively
τ = Shear stress,
f_{χ} = External force,
$\rho\frac{Du}{Dt}$ = Substantial time derivative of velocity,
u =Velocity vector in x direction

IV. BOUNDARY CONDITION AND GEOMETRY

In present analysis, an airfoil from the 6 series of NACA laminar wing section family is used. The airfoil maximum relative thickness is 21%, which is situated at 35% of the chord length. The Reynolds number taken for the simulation in the range of $x10^5$ and $x10^6$ and turbulence intensity is set at 10%. A turbulent flow solver is used in ANSYS Fluent, where spalart allmaras model is used. Calculation was performed for the "linear" region, i.e. for angles of attack (AOA) ranging from 4° to 8°, because of greater reliability of both computed and experimental values in this region. The selected airfoil profile has 50 no. vertices and it is created in ANSYS GUI with two edges upper and lower. The mesh is generated in ANSYS workbench and then boundary conditions are applied using ANSYS Fluent. Fig. 1 is showing the airfoil profile of NACA 63(4)-221.

Once the airfoil edges were created then boundary layers are generated around the airfoil. Meshed around airfoil at different angle of attack have shown from Fig. 2 to Fig. 5. The mesh generated is uniformly distributed around airfoil for accurate prediction.

V. CFD ANALYSIS OF AIRFOIL 63(4)-221 FOR 14 M HAWT BLADE USING ANSYS FLUENT

A. Preprocecessing

1) Preparation of CAD Model

2D CAD model of NACA airfoil 63(4)-221 is generated using ANSYS design modeler. Fig. 1 shows modelling of NACA airfoil 63(4)-221. Coordinates are shown in Table I named airfoil specification of NACA 63(4)-221 [4].

Table I. Airfoil specification of NACA 63(4)-221

Upper surface		**Lower surface**	
Station	**Ordinate**	**Station**	**Ordinate**
0.00000	0.0000	0.00000	0.00000
0.00367	0.01627	0.00633	-0.01527
0.00600	0.02001	0.00900	-0.01861
0.01075	0.02628	0.01425	-0.02414
0.02292	0.03757	0.02708	-0.03385
0.04763	0.05375	0.05237	-0.04743
0.07253	0.06601	0.07747	-0.05753
0.09753	0.07593	0.10247	-0.06559
0.14767	0.09111	0.15233	-0.07765
0.19792	0.10204	0.20208	-0.08612
0.24824	0.10946	0.25176	-0.09156
0.29860	0.11383	0.30140	-0.09439
0.34897	0.11529	0.35103	-0.09469
0.39934	0.11369	0.40066	-0.09227
0.44969	0.10949	0.45031	-0.08759
0.50000	0.10309	0.50000	-0.08103
0.55027	0.09485	0.54973	-0.07295
0.60048	0.08512	0.59952	-0.06370
0.65063	0.07426	0.64937	-0.05366
0.70071	0.06262	0.69929	-0.04318
0.75073	0.05054	0.74927	-0.03264
0.80067	0.03849	0.79933	-0.02257
0.85056	0.02693	0.84944	-0.01347
0.90039	0.01629	0.89961	-0.00595
0.95018	0.00708	0.94982	-0.00076
1.00000	0.00000	1.00000	0.00000
LE Radius: 0.0265, slope of radius through LE 0.0842			

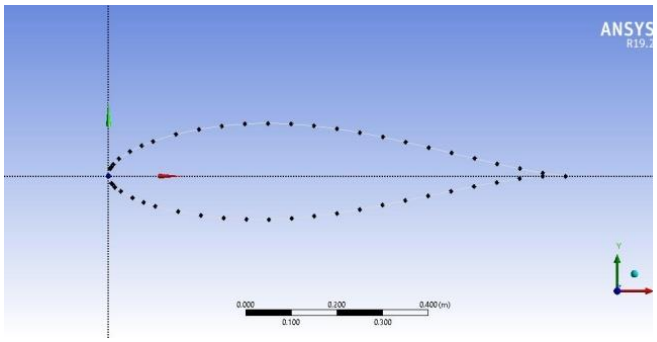

Fig. 1. Modelling of NACA airfoil 63(4)-221

2) Mesh Generation

Generate the mesh of airfoil in the Ansys mesh software. (Fig. 2 to Fig. 6 at different angle of attack). Table II shows variables taken for meshing around the airfoil.

Table II. Variables for meshing around airfoil

Mesh Type	Quadrilateral
No. of Nodes	90985
No. of Element	90259

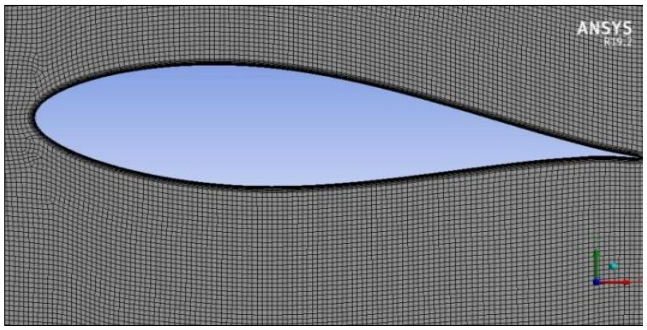

Fig. 2. Mesh around Airfoil-NACA 63(4)-221at AOA=4°

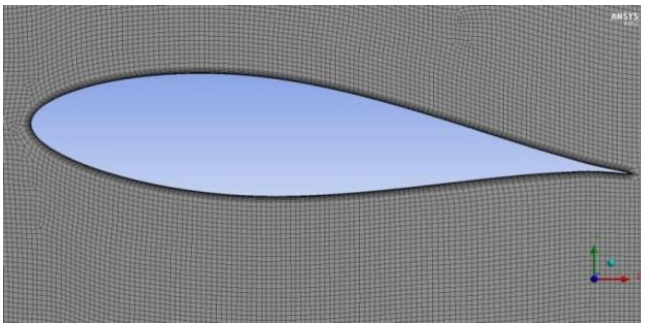

Fig. 3. Mesh around Airfoil-NACA 63(4)-221 at AOA=5°

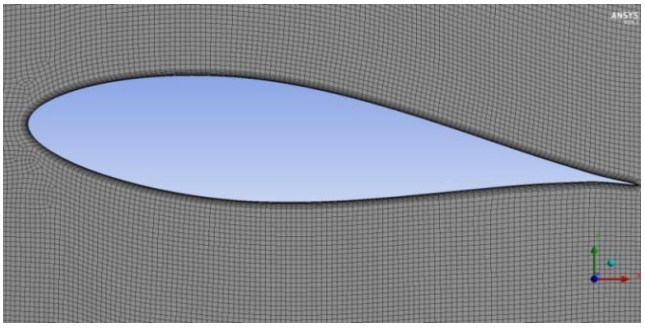

Fig. 4. Mesh around Airfoil-NACA 63(4)-221 at AOA=6°

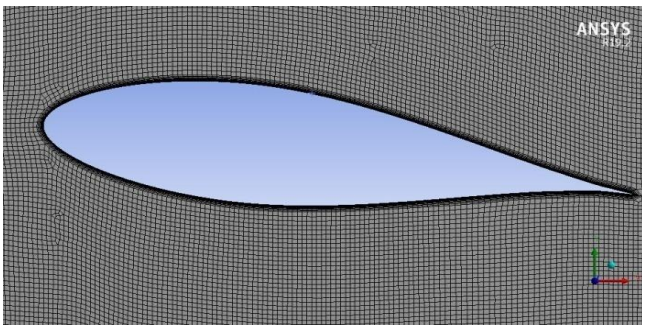

Fig. 5 Mesh around Airfoil-NACA 63(4)-221 at AOA=7°

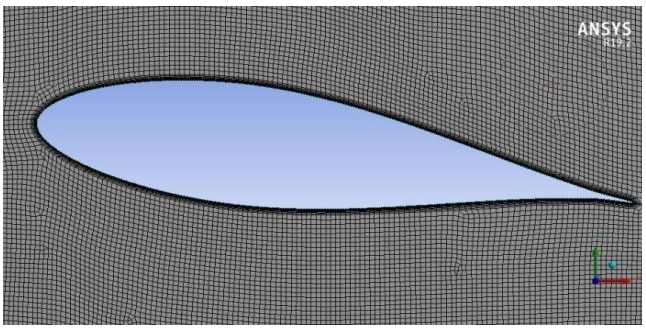

Fig. 6. Mesh around Airfoil-NACA 63(4)-221 at AOA=8°

3) Fluent Setup

After mesh generation define the following setup criteria in the ANSYS fluent as shown in Table III. Pressure outlet conditions are shown in Table IV.

Table III. Setup criteria

Problem Type	2D
Type of Solver	Pressure-based solver
Physical model	Viscous spalart allmaras (1 equation)
Material Property	Flowing fluid is air
Density of air	1.225 kg/m^3
Viscosity	1.7894e-05

Table IV. Pressure outlet condition

Gauge pressure	0 Pa
Turbulent viscosity ratio	10

B. Solution

1) Step 1-Solution Initialization

In this step Initialization of the solution is conduct to get the initial solution for the problem.

2) Step 2- Run Solution

Run the solution by giving 500 no of iteration for solution to converge. Following solution method is used for achieving solution (Table V).

Table V. Solution Method details

Pressure velocity coupling Scheme	COUPLED
Pressure	Second order upwind
Momentum	Second order upwind
Modified turbulence viscosity	First order

C. Post Processing

Post processing is performed for viewing and interpretation of the result. The result can be viewed in various formats like graph, value, animation etc. From Fig. 7 to 30 shows Pressure distribution, Velocity distribution and Velocity vector for selected airfoil at different wind velocity and angle of attack = 6°. These CFD results were also find out for other angle of attack as mention in Table VI and VII. In these tables lift force L, drag force D, lift coefficient C_l, drag coefficient C_d and C_l/C_d ratio is shown. It is clear from these results that angle of attack 6° give highest lift coefficient and C_l/C_d ratio. Values are shown in Table 6 and 7 for different Reynolds number in the range of 10^5 and 10^6 separately. Correction factor = 0.4 multiplied to drag coefficient, to get corrected drag coefficient as explained by (Ramanujam et al., 2016).

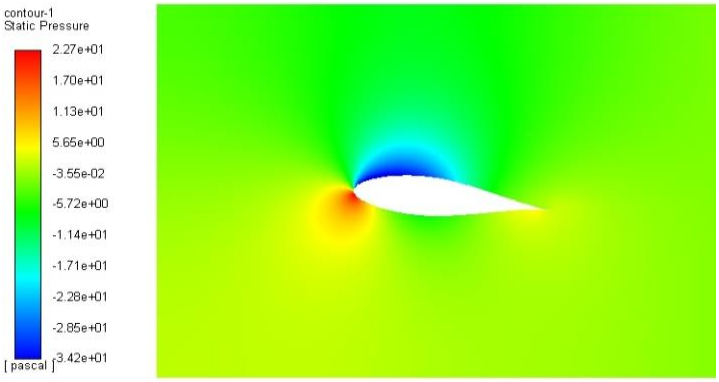

Fig. 7. Pressure distribution around Airfoil-NACA 63(4)-221 at AOA=6°and v=6 m/s

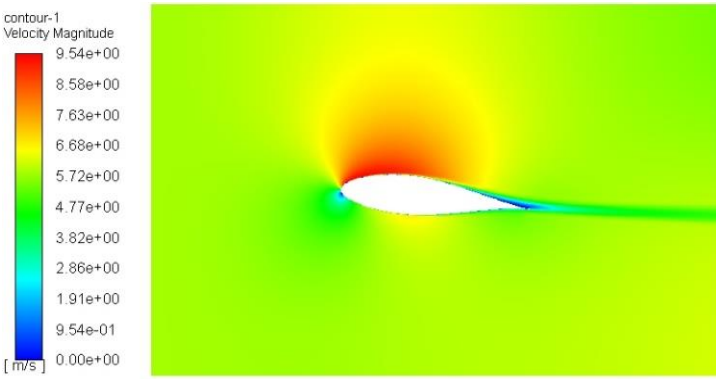

Fig. 8. Velocity distribution around Airfoil-NACA 63(4)-221 at AOA=6°and v=6 m/s

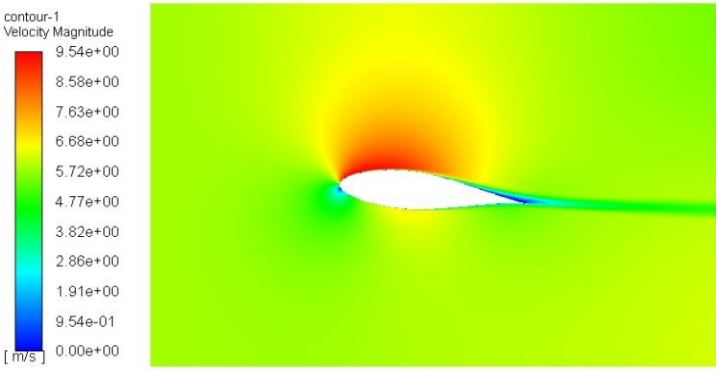

Fig. 9. Velocity vector around Airfoil-NACA 63(4)-221 at AOA=6°and v=6 m/s

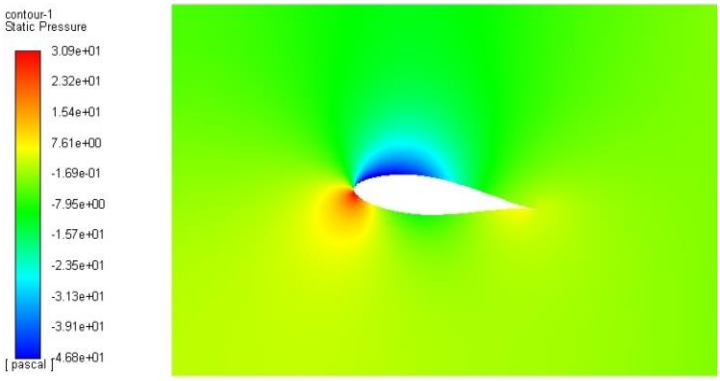

Fig. 10. Pressure distribution around Airfoil-NACA 63(4)-221 at AOA=6°and v=7 m/s

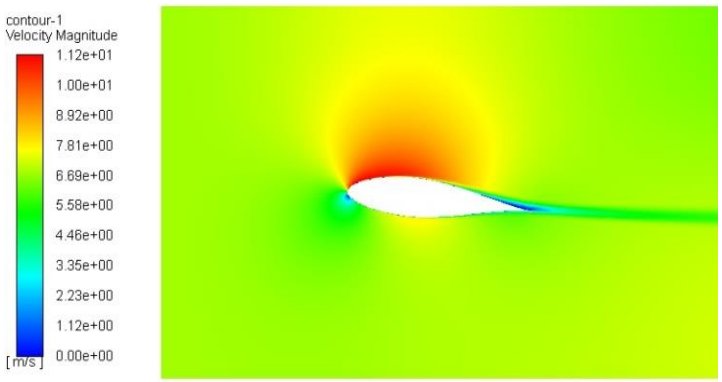

Fig. 11. Velocity distribution around Airfoil-NACA 63(4)-221 at AOA=6°and v=7 m/s

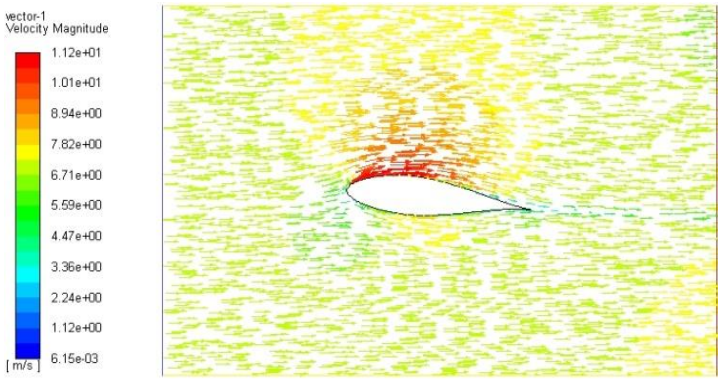

Fig. 12. Velocity vector around Airfoil-NACA 63(4)-221 at AOA=6° and v=7 m/s

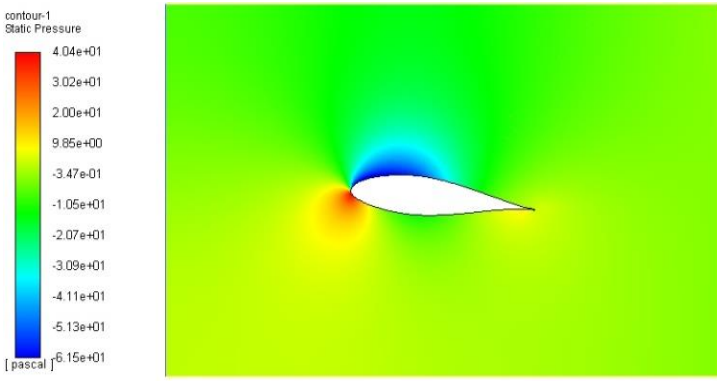

Fig. 13. Pressure distribution around Airfoil-NACA 63(4)-221 at AOA=6° and v=8 m/s

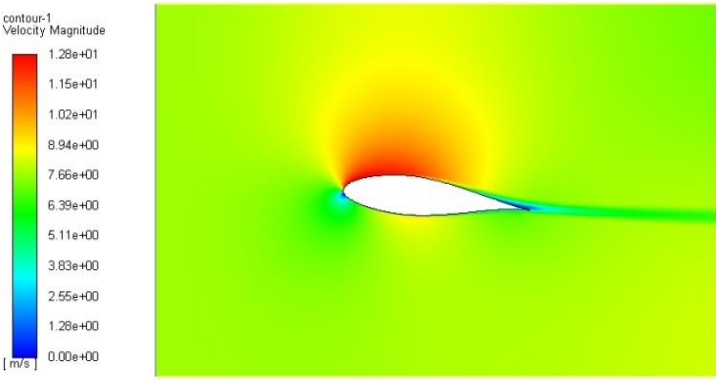

Fig. 14 Velocity distribution around Airfoil-NACA 63(4)-221 at AOA=6°and v=8 m/s

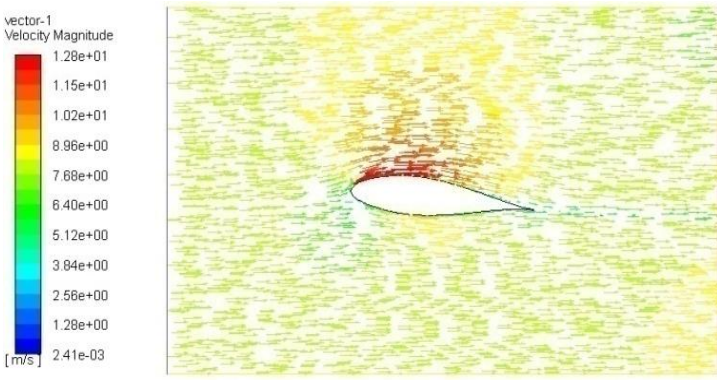

Fig. 15. Velocity vector around Airfoil-NACA 63(4)-221 at AOA=6°and v=8 m/s

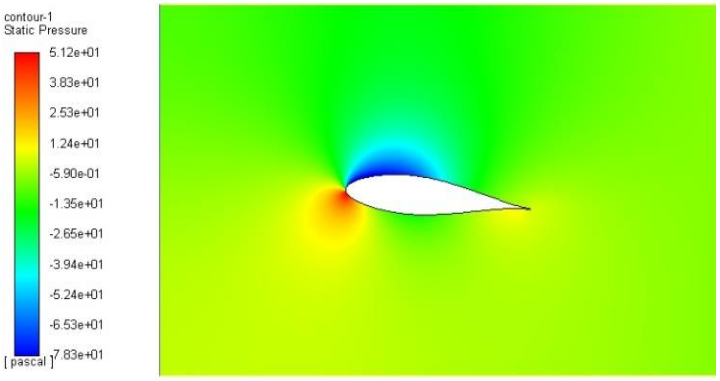

Fig. 16. Pressure distribution around Airfoil-NACA 63(4)-221 at AOA=6° and v=9 m/s

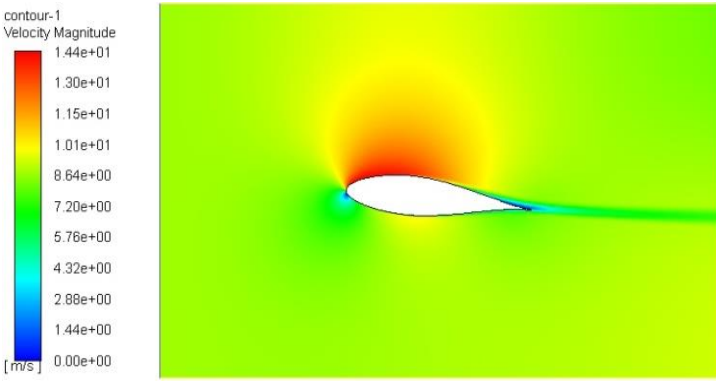

Fig. 17. Velocity distribution around Airfoil-NACA 63(4)-221 at AOA=6° and v=9 m/s

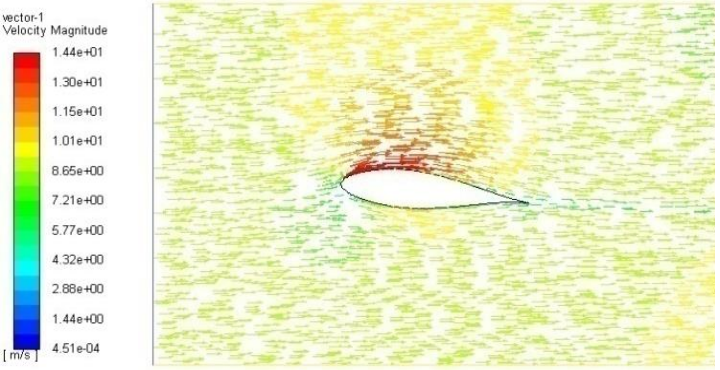

Fig. 18. Velocity vector around Airfoil-NACA 63(4)-221 at AOA=6° and v=9 m/s

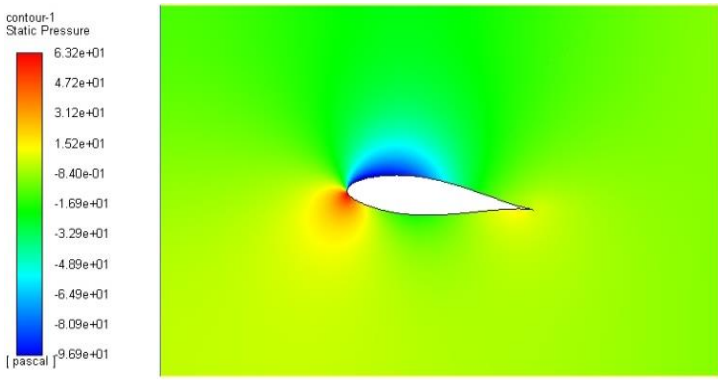

Fig. 19. Pressure distribution around Airfoil-NACA 63(4)-221 at AOA=6°and v=10 m/s

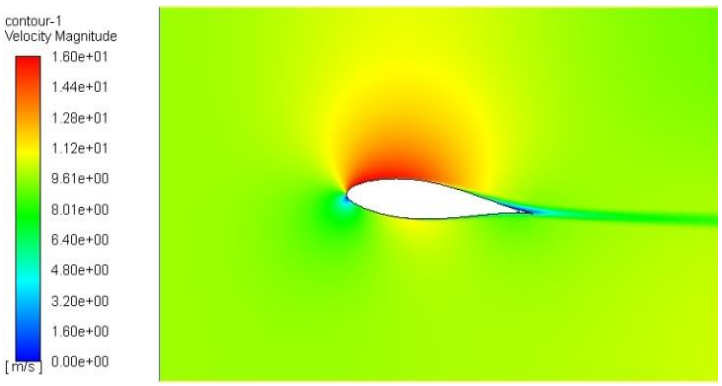

Fig. 20. Velocity distribution around Airfoil-NACA 63(4)-221 at AOA=6°and v=10 m/s

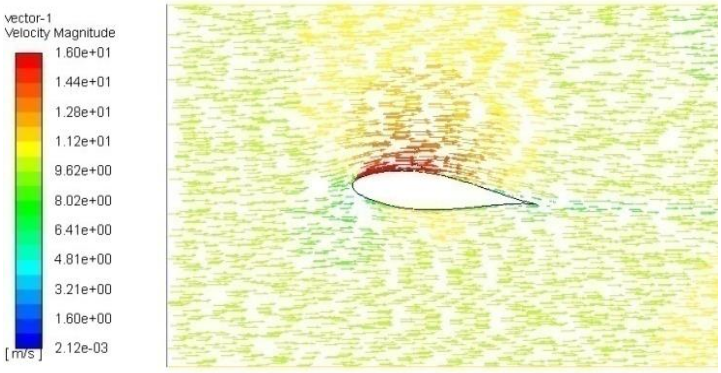

Fig. 21. Velocity velocity around Airfoil-NACA 63(4)-221 at AOA=6° and v=10 m/s

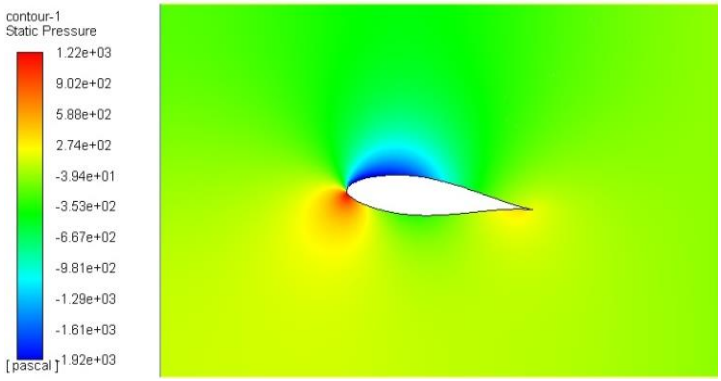

Fig. 22. Pressure distribution around Airfoil-NACA 63(4)-221 at AOA=6°and v=43.79 m/s

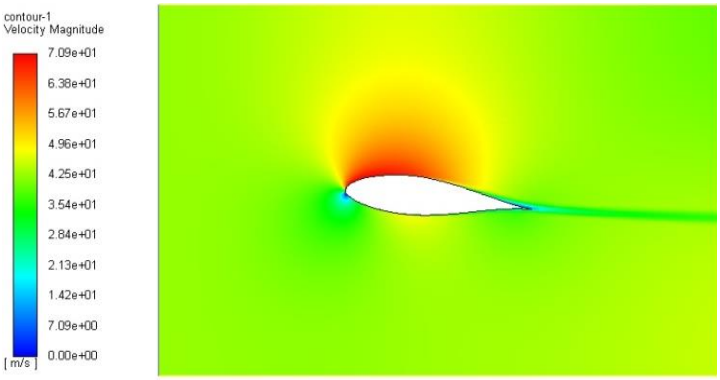

Fig. 23. Velocity distribution around Airfoil-NACA 63(4)-221 at AOA=6°and v=43.79 m/s

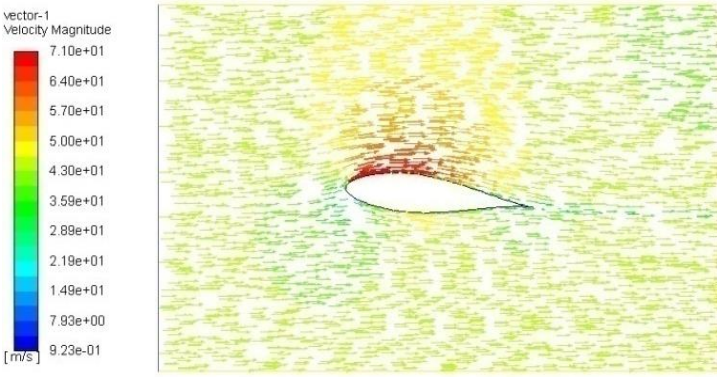

Fig. 24. Velocity vector around Airfoil-NACA 63(4)-221 at AOA=6°and v=43.79

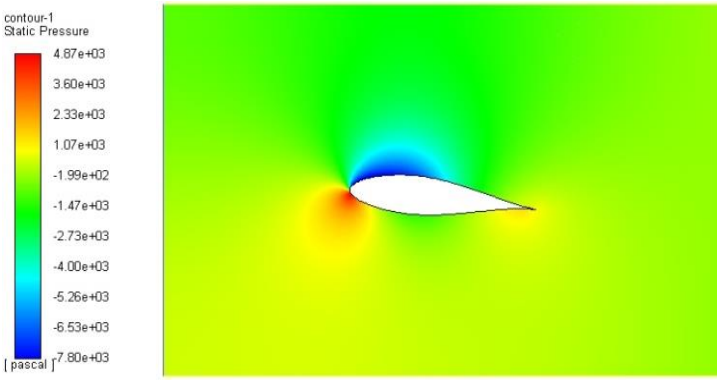

Fig. 25. Pressure distribution around Airfoil-NACA 63(4)-221 at AOA=6°and v=87.58 m/s

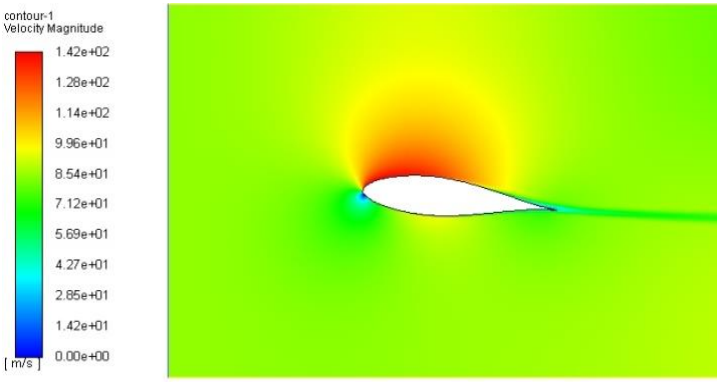

Fig. 26. Velocity distribution around Airfoil-NACA 63(4)-221 at AOA=6°and v=87.58 m/s

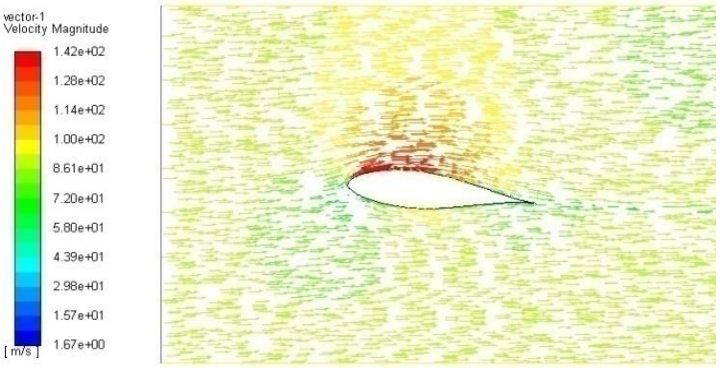

Fig. 27. Velocity vector around Airfoil-NACA 63(4)-221 at AOA=6°and v=87.58 m/s

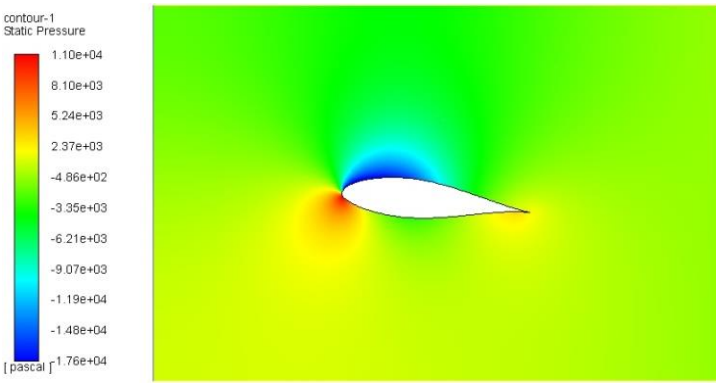

Fig. 28. Pressure distribution around Airfoil-NACA 63(4)-221 at AOA=6°and v=131.37 m/s

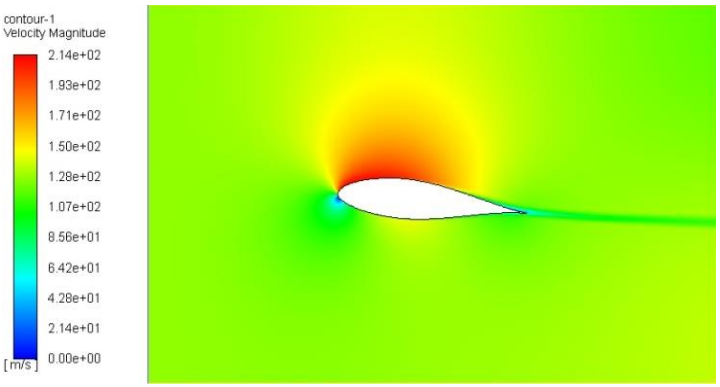

Fig. 29. Velocity distribution around Airfoil-NACA 63(4)-221 at AOA=6°and v=131.37 m/s

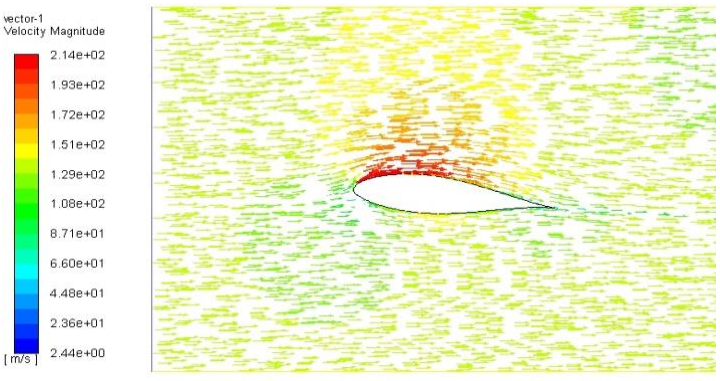

Fig. 30. Velocity vector around Airfoil-NACA 63(4)-221 at AOA=6°and v=131.37 m/s

Table VI. CFD analysis results of NACA airfoil 63(4)-221 at various angle of attack and wind speed for low Reynolds number (x 10^5)

Angle of attack (Degree)	Reynolds No.	Wind speed (m/s)	Drag force (N)	Drag Coefficient, C_d	Corrected drag coefficient, C_d	Lift force (N)	Lift coefficient, C_l	C_l/C_d ratio
4°	397061.74	6.0	0.48741	0.02210	0.00884	13.81279	0.62642	70.84730
4°	463238.70	7.0	0.63990	0.02132	0.00852	18.99529	0.63290	74.21159
4°	529415.66	8.0	0.81047	0.02067	0.00827	24.99530	0.63763	77.10047
4°	595592.61	9.0	1.00014	0.02015	0.00806	31.82257	0.64141	79.54481
4°	661769.57	10.0	1.21105	0.01977	0.00790	39.45804	0.64420	81.45355
5°	397061.74	6.0	0.53559	0.02428	0.00971	16.24221	0.73659	75.81421
5°	463238.70	7.0	0.70406	0.02345	0.00938	22.32535	0.74386	79.27356
5°	529415.66	8.0	0.89296	0.02277	0.00911	29.39745	0.74993	82.30328
5°	595592.61	9.0	1.10418	0.02225	0.00890	37.43394	0.75451	84.75457
5°	661769.57	10.0	1.33887	0.02185	0.00874	46.42601	0.75797	86.68825
6°	397061.74	6.0	0.59475	0.02697	0.01078	18.66507	0.84647	78.45724
6°	463238.70	7.0	0.78231	0.02606	0.01042	25.70568	0.85649	82.14612
6°	529415.66	8.0	0.99446	0.02536	0.01014	33.87317	0.86410	85.15458
6°	595592.61	9.0	1.23138	0.02481	0.00992	43.16754	0.87008	87.64042
6°	661769.57	10.0	1.49685	0.02443	0.00977	53.49336	0.87335	89.34293
7°	397061.74	6.0	0.66733	0.03026	0.01210	20.82543	0.94445	78.01681
7°	463238.70	7.0	0.87819	0.02926	0.01170	28.72091	0.95695	81.76109
7°	529415.66	8.0	1.11739	0.02850	0.01140	37.88486	0.96644	84.76180
7°	595592.61	9.0	1.38664	0.02794	0.01117	48.29977	0.97352	87.08039
7°	661769.57	10.0	1.68755	0.02755	0.01102	59.93634	0.97854	88.79193
8°	397061.74	6.0	0.75943	0.03444	0.01377	22.68052	1.02858	74.66238
8°	463238.70	7.0	0.99889	0.03328	0.01331	31.37178	1.04528	78.51610
8°	529415.66	8.0	1.27136	0.03243	0.01297	41.47370	1.05799	81.55338
8°	595592.61	9.0	1.57887	0.03182	0.01272	52.94724	1.06720	83.83720
8°	661769.57	10.0	1.92250	0.03138	0.01255	65.77964	1.07394	85.53898

Table VII. CFD analysis results of NACA airfoil 63(4)-221 at various angle of attack and wind speed for high Reynolds number (x 106)

Angle of attack	Reynolds No.	Wind speed (m/s)	Drag force (N)	Drag Coefficient, C_d	Corrected drag coefficient, C_d	Lift force (N)	Lift coefficient, C_l	C_l/C_d ratio
5°	3000000	43.79	21.35365	0.01817	0.00727	929.77072	0.79151	108.85381
5°	6000000	87.58	78.92014	0.01679	0.00671	3780.4004	0.80456	119.75397
5°	9000000	131.37	170.4888	0.01612	0.00645	8579.2665	0.81149	125.80395
6°	3000000	43.79	24.08764	0.02050	0.00820	1075.4018	0.91548	111.61343
6°	6000000	87.58	89.59506	0.01906	0.00762	4374.3581	0.93096	122.05913
6°	9000000	131.37	194.0922	0.01835	0.00734	9920.3236	0.93834	127.77846
7°	3000000	43.79	27.30909	0.02324	0.00929	1213.8412	1.03333	111.12058
7°	6000000	87.58	102.00160	0.02170	0.00868	4943.4744	1.05209	121.16169

7°	9000000	131.37	221.81895	0.02098	0.00839	11218.193	1.06111	126.43410
8°	3000000	43.79	31.22440	0.02658	0.01063	1352.3971	1.15129	108.28045
8°	6000000	87.58	117.45439	0.02499	0.00999	5528.5577	1.17661	117.67456
8°	9000000	131.37	255.76350	0.02419	0.00967	12557.665	1.18780	122.74684

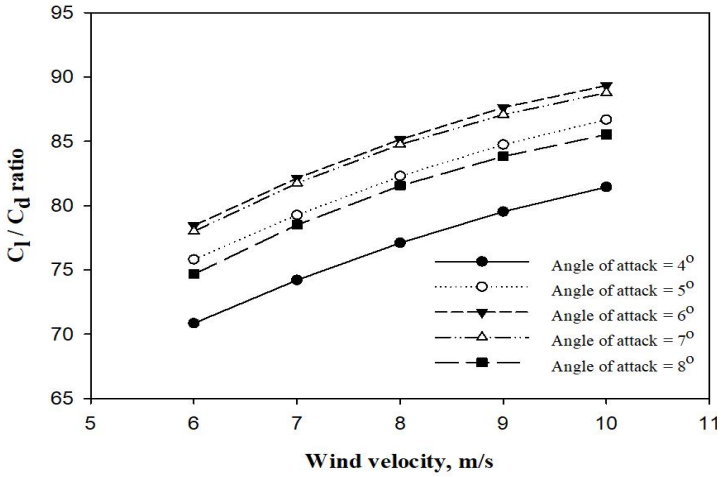

Fig. 12. C_l/C_d ratio at different angle of attack for different wind velocity at low Reynolds number (x 10^5)

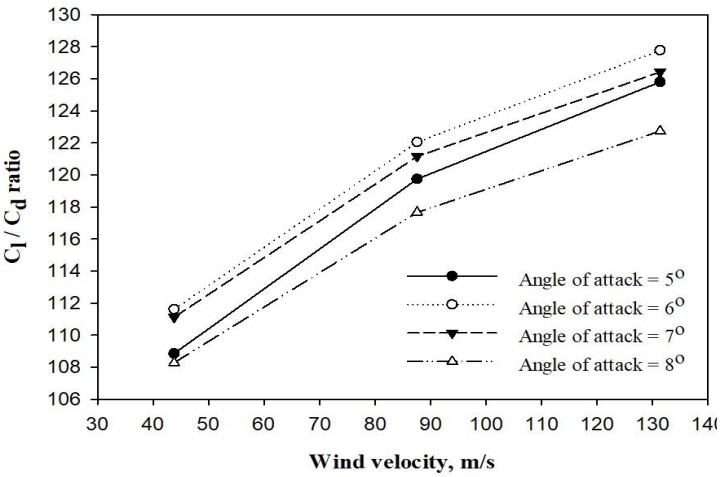

Fig. 13. C_l/C_d ratio at different angle of attack for different wind velocity at high Reynolds number (x 10^6)

VI. RESULTS

A. Pressure Distribution around Airfoil

The static pressure contour is shown in Fig. 7, 10, 13, 16, 19, 22, 25 and 28 for angle of attack 6 degree, because at this angle of attack C_l/C_d ratio is maximum as given Table VI and VII. The pressure at the bottom surface of airfoil for incoming flow is more than upper surface so the incoming air can effectively push the airfoil upward normal to flow direction of air.

B. Velocity Distribution around Airfoil

The Velocity distribution contour is shown in Fig. 8, 11, 14, 17, 20, 23, 26 and 29 for angle of attack 6 deg.

C. Velocity Vector around Airfoil

The Velocity vector contour is shown in Fig. 9, 12, 15, 18, 21, 24, 27 and 30 for angle of attack 6 deg.

D. Comparison of Simulation and Experimental Results

There are two forces and one moment works on an airfoil. The force component which is normal to the incoming flow stream is known as lift force and the component which is acting parallel to the flow stream is known as drag force. In this analysis, first of all simulation is carried out and then results are being verified with results available in previous literature. Here simulation is done for angle of attack 4° to 8°. Results shows the ratio lift coefficient to drag coefficient (C_l/C_d) increases with increasing angle of attack from 4° to 6° and then again decreasing with further increasing AOA. Hence AOA=6° shows maximum C_l/C_d ratio for both condition of low and high Reynolds number. This can be further use in blade design process. It is also find out that for any fix value of AOA, the C_l/C_d ratio increases with increasing wind velocity or increasing Reynolds. Lift coefficient also increases with increasing angle of attack 4° to 8° and Reynolds number, while drag coefficient decreases.

CONCLUSION

In this work CFD analysis of wind turbine blade is done in ANSYS Fluent. For this analysis spalart allmaras model is used for obtaining lift coefficient and drag coefficient at different angles of attack. The results obtained from simulation are compared with experimental results found in literature. It is found that sliding ratio is maximum at angle of attack = 6°. It is also found that the pressure at lower surface of airfoil is more and velocity is higher on the upper surface of airfoil.

ACKNOWLEDGEMENT

The authors would like to acknowledge the research support from the Rabindranath Tagore University, Bhopal, India.

REFERENCES

Anitha, D., Shamili, G., Ravi Kumar, P. and Sabari Vihar, R. (2018). Airfoil Shape Optimization Using Cfd And Parametrization Methods, *Materials Today: Proceedings*, 5(2), pp.5364-5373.

Bartl, J., Sagmo, K., Bracchi, T. and Sætran, L. (2019). Performance of the NREL S826 airfoil at low to moderate Reynolds numbers—A reference experiment for CFD models, *European Journal of Mechanics - B/Fluids*, 75, pp.180-192.

Bianchini, A., Balduzzi, F., Ferrara, G. and Ferrari, L. (2016). Aerodynamics of Darrieus Wind Turbines Airfoils: The Impact of Pitching Moment, *Journal of Engineering for Gas Turbines and Power*, 139(4).

Eggleston, D. and Stoddard, F. (1987). Wind Turbine Engineering Design, New York: Van Nostrand Reinhold.

Fuglsang, P., Bak, C., Gaunaa, M. and Antoniou, I. (2004). Design and Verification of the Risø-B1 Airfoil Family for Wind Turbines, *Journal of Solar Energy Engineering*, 126(4), pp.1002-1010.

Li, S., Zhou, D., Zhang, Y. and Qu, Q. (2015). Aerodynamic Investigation of RAE2822 Airfoil in Ground Effect, *Procedia Engineering*, 126, pp.174-178.

Md. Mehdi Masud Talukder, Md. Rukanuzzaman Rukan and Muhammed Kamrul Islam. (2016). "Comparative Aerodynamic Analysis of Wind Turbine Blade Profiles", *International Journal of Engineering Research*, V5(01).

Patil, B. and Thakare, H. (2015). Computational Fluid Dynamics Analysis of Wind Turbine Blade at Various Angles of Attack and Different Reynolds Number, *Procedia Engineering*, 127, pp.1363-1369. ysis of Blunt Trailing Edge Airfoils, *Journal of Solar Energy Engineering*, 125(4), pp.479-487.

Ramanujam, G., Özdemir, H. and Hoeijmakers, H. (2016). Improving airfoil drag prediction, *Journal of Aircraft*, 53(6), pp.1844-1852.

Standish, K. and van Dam, C. (2003). Aerodynamic analysis of blunt trailing edge airfoils. Journal of Solar Energy Engineering, 125(4), pp.479-487.

Sumit Sharma. (2016). An Aerodynamic Comparative Analysis of Airfoils for Low-Speed Aircrafts, *International Journal of Engineering Research*, V5(11).

Tenguria, N., Nigam, P., and Pradhan, M. (2017). Analysis of horizontal axis wind turbine blade using CFD, *International Journal of Engineering, Science and Technology*, 9(2), p.46.

Yang, H., Shen, W., Xu, H., Hong, Z. and Liu, C. (2014). Prediction of the wind turbine performance by using BEM with airfoil data extracted from CFD, *Renewable Energy*, 70, pp.107-115.

***